Journal of Magnetic Resonance 347 (2023) 107363

Contents lists available at ScienceDirect

Journal of Magnetic Resonance

journal homepage: www.elsevier.com/locate/jmr

A new ^{13}C trityl-based spin label enables the use of DEER for distance measurements

Zikri Hasanbasri [a], Martin Poncelet [b], Hannah Hunter [a], Benoit Driesschaert [b,c,*], Sunil Saxena [a,*]

[a] Department of Chemistry, University of Pittsburgh, Pittsburgh, PA 15260, United States
[b] Department of Pharmaceutical Sciences, School of Pharmacy & In Vivo Multifunctional Magnetic Resonance (IMMR) Center, Health Sciences Center, West Virginia University, Morgantown, WV 26506, United States
[c] C. Eugene Bennett Department of Chemistry West Virginia University, Morgantown, WV 26506, United States

ARTICLE INFO

Article history:
Received 4 November 2022
Revised 15 December 2022
Accepted 21 December 2022
Available online 30 December 2022

ABSTRACT

Triarylmethyl (TAM)-based labels, while still underutilized, are a powerful class of labels for pulsed-Electron Spin Resonance (ESR) distance measurements. They feature slow relaxation rates for long-lasting signals, high stability for cellular experiments, and narrow spectral features for efficient excitation of the spins. However, the typical narrow line shape limits the available distance measurements to only single-frequency experiments, such as Double Quantum Coherence (DQC) and Relaxation Induced Dipolar Modulation Enhancement (RIDME), which can be complicated to perform or hard to process. Therefore, widespread usage of TAM labels can be enhanced by the use of Double Electron-Electron Resonance (DEER) distance measurements. In this work, we developed a new spin label, $^{13}C_1$-mOX063-d_{24}, with a ^{13}C isotope as the radical center. Due to the resolved hyperfine splitting, the spectrum is sufficiently broadened to permit DEER-based experiments at Q-band spectrometers. Additionally, this new label can be incorporated orthogonally with Cu(II)-based protein label. The orthogonal labeling scheme enables DEER distance measurement at X-band frequencies. Overall, the new trityl label allows for DEER-based distance measurements that complement existing TAM-label DQC and RIDME experiments.

1. Introduction

Triarylmethyl (TAM)-based spin-labels have emerged as a powerful label for ESR-based distance measurements. These labels exhibit a general tris-(tetrathiaaryl)methyl core, shown in Fig. 1, where most of the spin density (>60 %) resides on the central carbon (C_1). Based on this motif a wide variety of labels have been synthesized [1–6]. TAM-based labels have narrow spectral features because the absence or small hyperfine interactions. The narrow lines can be efficiently excited by pulses [7], leading to up to thirty times higher signal intensity in pulsed ESR than commonly used and commercially available nitroxides [8]. In addition to the sensitivity, TAM labels have slow relaxation rates [9,10], even at room temperature, which have enabled a pathway towards distance measurements at physiological temperatures [11–15]. Finally, these TAM labels are highly resistant to reduction within cellular environments [16–18]. These advantages are desirable for ESR-based experiments in the field of structural biology. When a biomolecule is selectively labeled at a given site, ESR can measure site-specific dynamics of the molecule [19,20]. Furthermore, when two or more sites are labeled, ESR can measure distance constraints between spin-labels [21–27] on the biomolecule. More importantly, these measurements are not limited by protein size. Therefore, ESR can study large and complicated systems that are not easily studied using X-ray Crystallography or NMR. With the utility of ESR techniques, implementation of different types of spin-labels, such as Gd(III) [28–30], Mn(II) [31,32], Cu(II) [33–36], and especially TAM [8,14,37] expand the scope of critical biological questions that can be probed.

One of the limiting aspects of TAM-based labels is the available ESR techniques for TAM distance measurements. Specifically, only single-frequency pulsed-ESR techniques, such as Double Quantum Coherence (DQC) [21,22] or Relaxation-Induced Dipolar Modulation Enhancement (RIDME) [26,27] can be used due to the narrow spectral features of TAM. While DQC provides high-sensitivity TAM-based distance measurements, the method can be hard to implement on commercial instrumentation due to the need for short pulses and the long phase cycles needed to remove unwanted signals. Such large phase cycling procedures can often lead to long acquisition times on commercial instrumentation due to limited on-board phase cycling [38–41]. While TAM-based DQC have been successful [1,4,42–46], this technology is currently adopted only by

* Corresponding author.
E-mail addresses: benoit.driesschaert@hsc.wvu.edu (B. Driesschaert), sksaxena@pitt.edu (S. Saxena).

https://doi.org/10.1016/j.jmr.2022.107363
1090-7807/

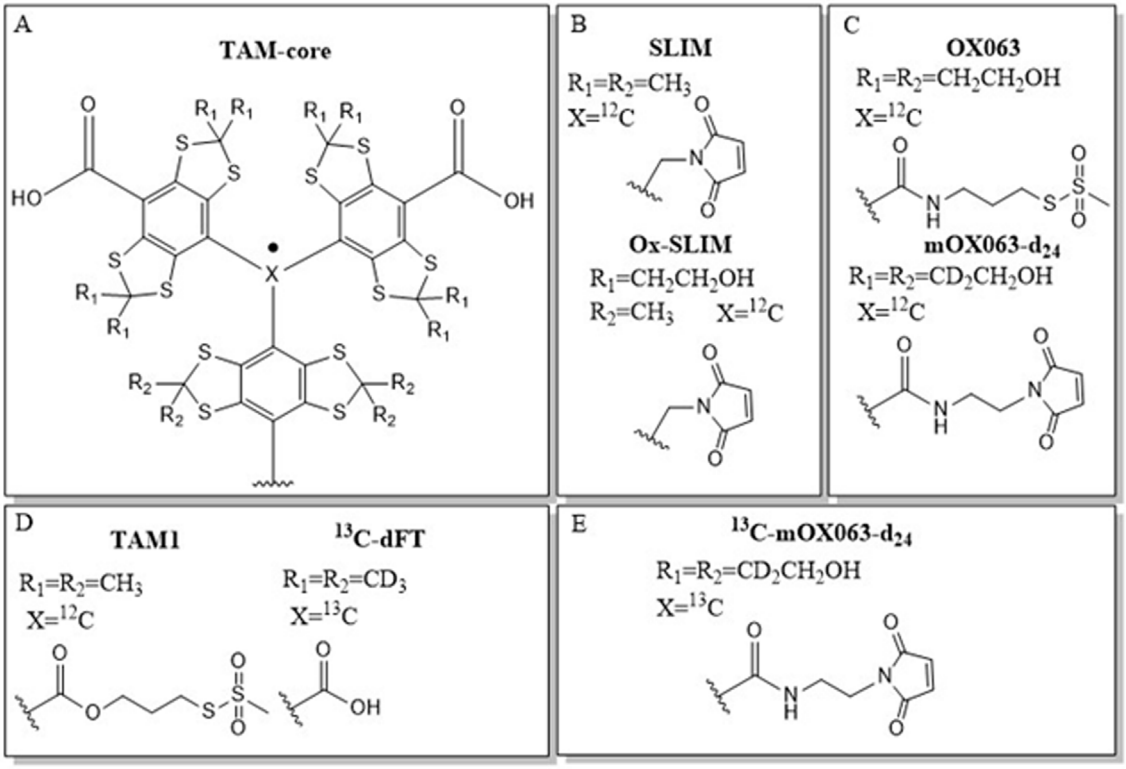

Fig. 1. A) Representation of the TAM-core. B) TAM-based labels that use Short Linker Maleimide (SLIM)[1,2]. C) Hydrophilic TAM-based labels with long linkers[3,4]. D) Hydrophobic TAM-based labels[5,6]. E) New label derived from mOX063-d_{24} with ^{13}C isotope as the radical center.

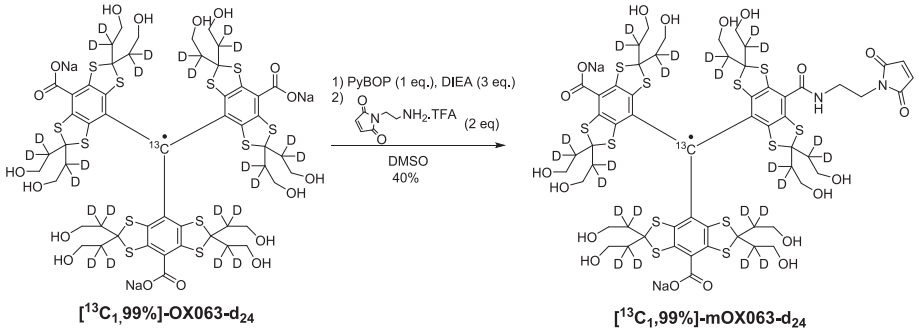

Scheme 1. Synthesis of $^{13}C_1$-mOx063-d_{24}.

a select few researchers. On the other hand, RIDME can also provide sensitive TAM-based distance measurements. However, RIDME suffers from the complex background signal [47]. Moreover, the distance distribution can be analyzed only after the background is subtracted correctly using various methods [48]. With these considerations, expanding the available pulsed-ESR technique to include a two-frequency technique, Double Electron-Electron Resonance (DEER) [23,24], will further improve the accessibility of TAM-based labels.

To date, DEER on TAM radicals has been performed under three conditions. The first condition is when TAM distances were obtained at high frequencies, i.e at W-band [49,50] or G-band [45]. With higher frequencies, the TAM spectrum is broad enough to allow the observer frequency and pump frequency to be at a reasonable frequency separation. The second condition is at Q-band frequency where the observer was set at the edge of the TAM spectra. This choice of observer frequency reduced the sensitivity of the measurement by sevenfold when compared to DQC measurements [42]. In the last case, DEER was done on TAM by exciting a set of ^{13}C present at natural abundance in the label [51]. These results suggest that the spectra of current TAM-based labels are too narrow at the commonly available X- and Q- band spectrometer frequencies. One solution to this problem is to have a TAM label with resolved splitting at commonly available frequencies.

Recently, a TAM radical with a ^{13}C isotope as the radical center, shown in Fig. 1D, was synthesized and shown to be sensitive to viscosity [5]. The ^{13}C isotope leads to a resolved splitting due to a hyperfine interaction with the ^{13}C nuclear spin (I = 1/2). This spectral feature due to ^{13}C can make the TAM radical well suited for DEER distance measurements that require pulses at two separate frequencies. Therefore, distance measurements will benefit from incorporation of $^{13}C_1$ into previously published TAM-based labels. For example, we previously showed that hydrophilic mOX063-d^4_{24}, shown in Fig. 1C, labels proteins with high efficiency and is cleavage-resistant protein labeling in-cells. Furthermore, the hydrophilic nature of mOX063-d_{24} provides long relaxation times

which allowed for distance measurements to be performed at 150 K and in-cell. In particular, the hydrophilicity reduces lipophilic interactions that enhances the relaxation times of the label[3].

In this work, we developed a new TAM label, $^{13}C_1$-mOX063-d_{24}, as shown in Fig. 1E, for DEER distance measurements. First, we show that the $^{13}C_1$-mOX063-d_{24} can label the intended labeling site efficiently. Next, we demonstrate that the spectral breadth of $^{13}C_1$-mOX063-d_{24} allows for DEER distance measurements at Q-band. Finally, we implement $^{13}C_1$-mOX063-d_{24} in an orthogonal labeling scheme with a Cu(II)-based label at X-band for DEER measurements. Overall, we showcase the power of $^{13}C_1$-mOX063- d_{24} and expand the ESR techniques available for TAM-based distance measurements.

2. Methods

2.1. Synthesis of [$^{13}C_1$, 99 %]-mOX063-d_{24}

The synthetic scheme for the spin label is shown in Scheme 1. Briefly, [$^{13}C_1$, 99 %]-OX063-d_{24} trisodium salt synthesized using known protocols [52], (300 mg, 0.21 mmol, 1 eq.) was dissolved in 10 mL of DMSO under argon. Diethylisopropylamine (DIEA) (108 μL, 0.62 mmol, 3 eq.) was added to the solution, followed by Benzotriazol-1-yl-oxytripyrrolidinophosphonium hexafluorophosphate (PyBOP) (107 mg, 0.21 mmol, 1 eq.). The green solution turned red and was stirred for 30 min. Then, N-(2-aminoethyl)maleimide trifluoroacetate salt (105 mg, 0.42 mmol, 2 eq.) was added, and the reaction was stirred at room temperature for 90 min. The reaction mixture was diluted with 500 mL of water containing 0.1 % trifluoroacetic acid (TFA). The product was loaded on a C18 column and purified using a gradient of water and acetonitrile (ACN) both containing 0.1 % TFA, from 5 % ACN to 15 % ACN, using a Teledyne CombiFlash Rf + system. The purified product was freeze-dried, then the resulting brown powder was dissolved in deionized water and titrated to pH = 7 with sodium hydroxide. The solution was freeze-dried again, affording 128 mg (40 %) of [$^{13}C_1$,99 %]-mOX063-d_{24} as a green powder named $^{13}C_1$-mOX063-d_{24} thorough the manuscript. The purity was evaluated to > 98 % by HPLC/MS (Figure S1).

2.2. GB1 labeling protocol

Expression and purification of E15C/K28C or E15C/K28H/Q32H GB1 mutants were performed as previously described [53]. The protein was incubated overnight at 4 °C in the presence of tris(2-carboxyethyl)phosphine (TCEP) to reduce any disulfide bonds. TCEP was removed by flowing the solution through GE Healthcare Hitrap desalting columns directly into a solution of $^{13}C_1$-mOX063-d_{24}. The labeling reaction occurs overnight at 4° C with the ratio of $^{13}C_1$-mOX063-d_{24}:GB1 being 10:1. After incubation, the solution was dialyzed for 72 h using a 2-kDa MW cutoff Spectra/Por7 Dialysis Membrane in PBS pH 6.8 to remove unreacted labels. The dialyzed solution was concentrated using Amicon Ultra Centrifugal Filter Units with a 3-kDa cutoff. UV–vis measurement using Nanodrop2000 Spectrophotometer from Thermo Scientific was used to determine concentration and labeling efficiency, as previously described[4].

For Cu(II) labeling, a 10 mM stock of Cu(II) chelated by nitrilotriacetic acid (NTA) was prepared as described previously [34,54,55]. The $^{13}C_1$-mOX063-d_{24} labeled GB1 was added with Cu(II)NTA in a 1:1 ratio, and the mixture was incubated at 4° C for 30 min. The samples were prepared in 3-*N*-morpholinopropanesulfonic acid (MOPS) buffer to allow efficient Cu(II)NTA binding to the dHis motif [55]. After incubation, 40 % deuterated glycerol was added, and the sample was flash-frozen with liquid MAP-Pro Propylene/propane gas. The Cu(II)NTA spin-labeling and freezing process followed a step-by-step protocol published recently [54].

2.3. ESR measurements

Room-temperature continuous-wave (CW)-ESR were performed on a Bruker ElexSys E680 CW/FT X-band spectrometer with a Bruker ER4122 SHQE-W1 resonator. Capillary tubes were used to hold the CW ESR samples. For $^{13}C_1$-mOX063-d_{24}, the experiments used the following parameters: center field of 3520 G, sweep width of 100 G, frequency of ~9.87 GHz, modulation amplitude of 0.5 G, modulation frequency of 100 kHz, data points of 2048, and conversion time of 40.00 ms. For Cu(II)NTA, the experiments used the following parameters: center field of 3200 G, sweep width of 2000 G, frequency of ~ 9.65 GHz, modulation amplitude of 4 G, modulation frequency of 100 kHz, data points of 1024, and conversion time of 20.48 ms.

For low-temperature experiments, an Oxford CF935 dynamic continuous-flow cryostat attached to Oxford LLT 650 low-loss transfer tube and Oxford ITC503 temperature controller ensured stable cryogenic temperature of the samples.

A three-pulse electron-spin echo envelope modulation (ESEEM) sequence [56,57], $(\pi/2)-t_1-(\pi/2)-t_2-(\pi/2)$, were performed at 18 K at X-band. The period t_1 was set as 140 ns. Additionally, t_2 was incremented in steps of 16 ns for a total of 1024 points from an initial value of 280 ns. The experiment was done at the field with the highest Cu(II)NTA echo intensity. A four-step phase cycling was used to eliminate the undesired echoes [58]. The resulting time domain was transformed into the frequency domain using Fast Fourier Transform. The magnitude of the spectrum from 0 MHz to 10 MHz is shown in the Results and Discussion section.

Q-band DEER was performed using a four-pulse sequence, $(\pi/2)\upsilon_A$-t_1-$(\pi)\upsilon_A$-$(t_1+\tau)$-$(\pi)\upsilon_B$-$(t_2-\tau)(\pi)\upsilon_A$. The pump ($\upsilon_B$) and observer ($\upsilon_A$) frequencies were set respectively at the first and second local maximum of the $^{13}C_1$-mOX063-d_{24} spectra. The periods t_1 and t_2 were set as 400 ns and 3200 ns, respectively. The parameter τ was increased by increments of 16 ns for a total of 166 time points. A 16-step phase cycling was implemented to obtain the main DEER echo[24]. For X-band DEER, all parameters are the same except for υ_A and υ_B, which were set respectively at the first local maxima of the $^{13}C_1$-mOX063-d_{24} spectra and the maximum of the Cu(II)NTA spectra.

All X-band pulsed experiments were performed on Bruker ElexSys E680 X-band FT/CW spectrometer using Bruker EN4118X-MD4 resonator and a 1 kW amplifier, while Q-band experiments used Bruker ElexSys E580 CW/FT X-band spectrometer using a Bruker ER5106-QT2 resonator for Q-band and a 300 W amplifier.

3. Results and Discussion

In this work, we used the immunoglobulin binding domain of protein G (GB1). Specifically, we engineered and overexpressed a double cysteine mutant E15C/K28C GB1 [59,60]. The protein was labeled with $^{13}C_1$-mOX063-d_{24} at both cysteine residues of GB1, as described in the Methods section. In summary, E15C/K28C-GB1 was incubated with ten times the excess amount of label to cysteine residues at 4° C for 16 h. After the reaction, the unreacted label was removed through dialysis. The dialyzed sample was then concentrated using centrifugal filter units.

To assess the labeling efficiency, we quantified the concentrations of protein and spin-label using UV–vis, as shown in Fig. 2A. The UV–vis spectrum of the sample is a sum of the spectrum of GB1 and $^{13}C_1$-mOX063-d_{24}. Therefore, we can obtain the concen-

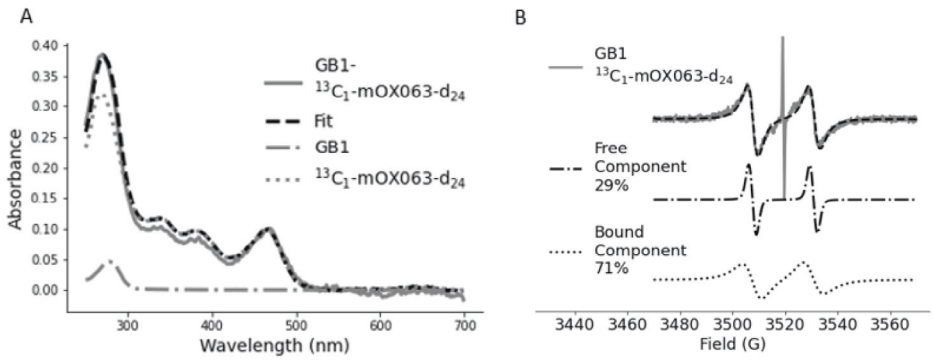

Fig. 2. A) UV–vis spectrum of $^{13}C_1$-mOX063-d_{24}-GB1 sample (gray line). The $^{13}C_1$-mOX063-d_{24}-GB1 spectra can be fitted by the sum of its GB1 (dash-dotted line) and $^{13}C_1$-mOX063-d_{24} (dotted line) components. B) CW-ESR spectrum of $^{13}C_1$-mOX063-d_{24}-GB1 (top). The spectrum of $^{13}C_1$-mOX063-d_{24}-GB1 can be fit using a two-component simulation using EasySpin[61]. Each component has a peak-to-peak linewidth of 1.4 G and 3.6 G for the free and bound components, respectively.

tration of both protein and label by fitting the sample spectra with the spectra of the protein and label individually, as described previously[4]. By using the extinction coefficient of GB1 ($\epsilon_{280} = 9970 cm^{-1}M^{-1}$) and $^{13}C_1$-mOX063-d_{24} ($\epsilon_{470} = 16219 cm^{-1}M^{-1}$, cf. Figure S2), we calculated the final concentrations of GB1 and the label in the sample to be 71 μM and 202 μM, respectively. Therefore, the ratio of cysteine:$^{13}C_1$-mOX063-d_{24} in our sample is 1:1.4, which may be due to incomplete removal of our unreacted label after dialysis.

With the unreacted label in our sample, we performed continuous wave (CW)-ESR at room temperature to quantify the amount of bound and free label, shown in Fig. 2B. The spectrum, shows a doublet pattern that originate from the hyperfine interaction with the $^{13}C_1$ nuclear spin (I = 1/2)[5]. In addition, a sharp peak at the center of the spectrum $\sim$ 3520 G arise from the 1 % isotopologue of the label having a ^{12}C at the central carbon, as the label was labeled 99 % $^{13}C_1$.

Using EasySpin [61], we simulated the room temperature CW-ESR spectrum, using a sum of two components. Both components had the same g_x, g_y, and g_z of 2.0033, 2.0032, and 2.0027, respectively while A_x, A_y, and A_z were 18 MHz, 18 MHz, and 160 MHz, respectively, as reported for $^{13}C_1$-OX063-d_{24} [52]. The only difference between the two components is the rotational correlation time (τ_r). The first component has a τ_r of 0.55 ns while the second component has a τ_r of 1.80 ns. In the simulations, we assumed isotropic tumbling since the spectral lineshape for this system is largely insensitive to anisotropic tumbling (cf. Figure S3). The first component corresponds to the free label, as its rotational correlation time matches τ_r determined for the free $^{13}C_1$-mOX063-d_{24} (cf Figure S4) under similar conditions. Therefore, the sample contains $\sim$ 29 % of free label and 71 % of bound label. Spin-counting of the spectra provides a total of 205 μM of spins, which agrees with the concentration obtained from UV–vis. More importantly, the fitting indicates that 145 μM of the labels are bound, which matches the concentration of 142 μM cysteines in our sample. This labeling efficiency is consistent with the documented labeling efficiency of mOX063-d_{24}[4], which is an isotopologue of our new $^{13}C_1$-mOX063-d_{24} label. Overall, $^{13}C_1$-mOX063-d_{24} can efficiently label GB1.

Despite efficient labeling, the free label can still affect the sensitivity of subsequent distance measurements. Repetition of the sample preparation still contained some between 21 % and 34 % free label. The incomplete removal of the free label is due to the 2 kDa MW cutoff of the dialysis tubing, whose size was limited by the 6.2 kDa GB1 and the 1.5 kDa $^{13}C_1$-mOX063-d_{24}. As a result, the diffusion rate of the label is significantly slow during dialysis, leading to incomplete label removal even after 72 h. On the other hand, large MW cutoff can easily remove free label, as shown in Figure S5. Therefore, filtering free $^{13}C_1$-mOX063-d_{24} in larger protein systems is expected to be easier since the MW cutoff can be larger than what is used in this work.

Next, we obtained a Q-band Field-Swept Electron Spin Echo (FS-ESE) spectrum at 40 K. The data is shown in Fig. 3A. As a comparison, the FS-ESE spectra of mOX063-d_{24} is overlaid on the FS-ESE spectrum of $^{13}C_1$-mOX063-d_{24}-labeled GB1 sample in Fig. 3B. The spectrum of $^{13}C_1$-mOX063-d_{24} is ca. fivefold wider than mOX063-d_{24}. The breadth of the $^{13}C_1$-mOX063-d_{24} spectrum is expected from the 160 MHz value of A_z [52]. Additionally, the spectrum exhibit two central peaks separated by the $A_x = A_y$ of 18 MHz [52]. More importantly, the $^{13}C_1$-mOX063-d_{24} spectrum is wide enough for two frequencies separated by $\sim$ 100 MHz to excite different populations of the label. This result suggests an easy implementation DEER where the observer frequency is set at one peak while the pump frequency is set at the other. In contrast, the same 100 MHz separation cannot fit within the narrow spectra mOX063-d_{24}. Overall, the new $^{13}C_1$-mOX063-d_{24} label is well-suited for DEER distance measurements.

We performed Q-band DEER on the $^{13}C_1$-mOX063-d_{24}-labeled GB1 sample, shown in Fig. 4. The time-domain signal was analyzed using Consensus DEER Analysis (CDA) [63,64], which allows for analysis with minimal user bias. Additional information on relaxation rate measurements and fitting analysis is described in ESI. The corresponding distance distribution is shown in Fig. 4B, with the most probable distance at 3.6 nm. As a comparison, we overlaid a distance distribution obtained from *in silico* mOX063-d_{24} modeling, which was implemented into MTSSLWizard [65], as described previously [4]. The program randomly generates different rotamers of the label on GB1 and selects those conformations that do not clash with the protein. Fig. 4B, shows that the experimental distance distribution is in reasonable agreement with the predicted distribution. Additionally, the most probable distance is consistent with the distance obtained on the same mutant from DQC measurements on mOX063-d_{24} labeled protein [4].

In addition to the distance distribution, we also observed a 16 %$\pm$1% modulation depth (λ) from the time-domain signal. To understand the λ, we obtained the probability of exciting the spins from the pump pulse (p_b), as previously described [33,34,55,66–69]. In summary, p_b can be quantified by dividing the area of the spectra excited by our 16 ns pump pulse by the total area of the spectra, leading to p_b of 30.9 %. Given that λ can be expressed as [68]:

$$\lambda = p_b \times f_2 \quad (1)$$

where f_2 is the fraction of doubly-labeled species in our sample. From the UV–vis and room temperature CW-ESR data shown in Fig. 2, we estimate 71 μM of doubly-labeled GB1 and 60 μM of free

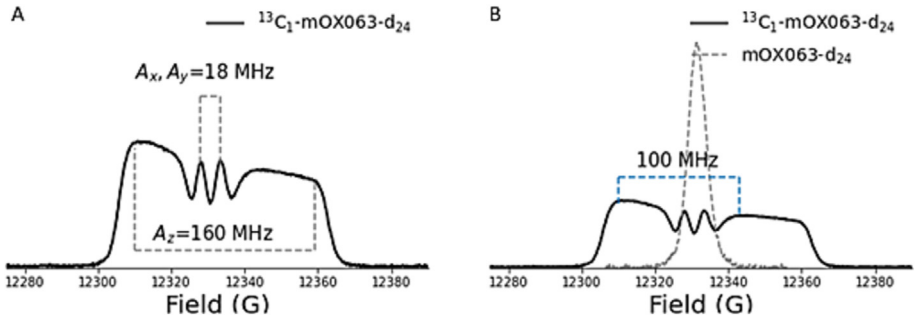

Fig. 3. A) Field-swept (FS) spectrum of $^{13}C_1$-mOX63-d_{24} at 40 K. The gray dashed lines represent peak separations that correspond to the different hyperfine values of the label. B) Field-swept (FS) spectrum of $^{13}C_1$-mOX63-d_{24} and mOX063-d_{24} at 40 K. The blue dashed lines indicate the frequency separation between the two local maxima of the $^{13}C_1$-mOX063-d_{24} spectra.

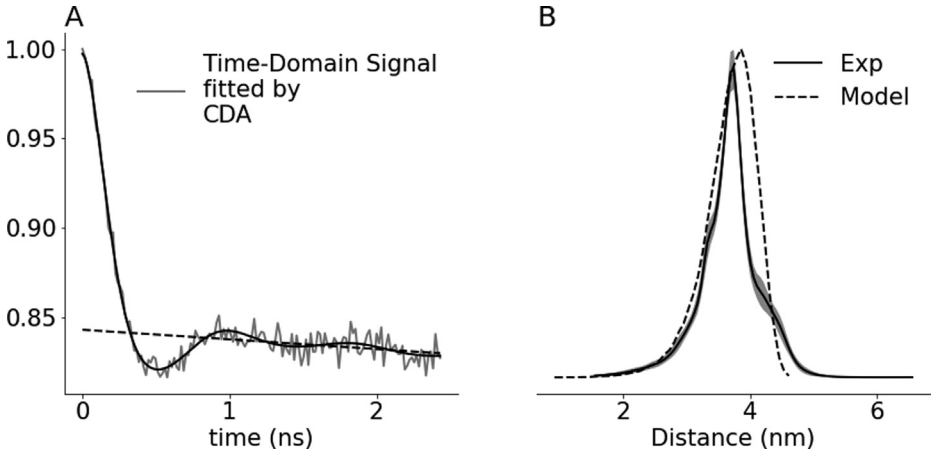

Fig. 4. A) Q-band DEER signal of $^{13}C_1$-mOX063-d_{24}-GB1. The background signal is shown by dashed line. B) The distance distribution (solid line) of $^{13}C_1$-mOX063-d_{24}-GB1 and the modeled distance (dashed line). The analysis was done using ComparativeDEERAnalyzer (CDA) [63,64]. Modeling the conformational space of $^{13}C_1$-mOX063-d_{24} was done using MTSSLWizard [65], as described previously[4].

label that forms the 'singly-labeled' species in our sample. These concentrations translate into f_2 and f_1 of 53.8 %± 0.5 % and 46.2 %±0.5%, respectively. Based on Eq. (1), we expected λ to be 16.6 %± 0.2 % which is within the error of our experimental λ of 16 %± 1 %. Overall, the results support a high labeling efficiency.

The Q-band $^{13}C_1$-mOX063-d_{24} DEER experiment showcases the utility of the new spin-label for DEER distance measurements. However, $^{13}C_1$-mOX063-d_{24} DEER is not as sensitive as the typical TAM-based DQC experiments. Specifically, the modulation depth from $^{13}C_1$-mOX063-d_{24} DEER is lower than the 80 % to 100 % modulation depth of DQC [43]. The sensitivity of TAM-based DQC enables distance measurements on samples with concentration as low as 45 nM [1]. Despite the sensitivity disadvantage of $^{13}C_1$-mOX063-d_{24} DEER experiments are easier to perform than DQC. Specifically, DEER only requires 2 to 16-step phase cycles [24] to isolate the proper DEER echo, while optimally DQC requires a 256-step phase cycle [22] to obtain the correct DQC echo. The extensive phase cycling in DQC is essential as incomplete removal of unwanted echoes can lead to artifacts in the time-domain signal [4]. Therefore, the new $^{13}C_1$-mOX063-d_{24} complements other TAM-based labels by providing the option of accessible DEER experiments.

Next, we explored the use of $^{13}C_1$-mOX063-d_{24} in an orthogonal-labeling scheme with a Cu(II)-based label, dHis-Cu(II) [35]. To achieve orthogonal labeling, we engineered and overexpressed an E15C/K28H/Q32H GB1 mutant. The protein was labeled with $^{13}C_1$-mOX063-d_{24} at the E15C residue of GB1, while Cu(II)NTA was coordinated to the K28H/Q32H residues (dHis motif). The use of Cu(II) chelated to nitrilotriacetic acid (NTA) [34] reduces non-specific binding and promotes selectivity to the dHis motif. Because Cu(II)NTA and our TAM-based labels have different labeling chemistry, selective labeling of the protein is facile [70].

We assessed Cu(II)NTA labeling of GB1 using 80 K CW-ESR and three-pulse Electron Spin Echo Envelope Modulation (ESEEM) [58], as shown in Fig. 5. We simulated the 80 K CW-ESR spectrum, shown in Fig. 5A, using the $g_{||}$ and $A_{||}$ parameters listed in Table S1. Compared with g and hyperfine tensors of free Cu(II) NTA, the value of $g_{||}$ decreases while the value of $A_{||}$ increases in the presence of GB1 mutant, consistent with the expected desolvation and coordination to the dHis motif [33–35]. Histidine coordination is further supported in the ESEEM time-domain signal, shown in Fig. 5B. Fourier transform of the time domain depicts signal at ~ 0.5, ~1, and ~ 1.5 MHz corresponding to Nuclear Quadrupole Interaction peaks and ~ 4.5 MHz corresponding to Double Quantum peaks [71]. These peaks are the signature of histidine coordination with Cu(II) [72]. Since the equivalence of added Cu (II)NTA to GB1 is 1:1 (50μ M:50μ M), we expect 98 % labeling efficiency based on the reported binding affinity of dHis-Cu(II) [70]. Overall, the single-component CW-ESR and ESEEM reveal efficient labeling of Cu(II)NTA to GB1.

After establishing the labeling of dHis-Cu(II) and $^{13}C_1$-mOX063-d_{24}, we performed an X-band DEER experiment at 40 K of the orthogonally-labeled GB1 sample, shown in Fig. 6. The DEER could only be performed at X-band frequency where the separation between the Cu(II)NTA spectra and $^{13}C_1$-mOX063-d_{24} is within the resonator bandwidth. The FS-ESE spectrum, shown in the inset

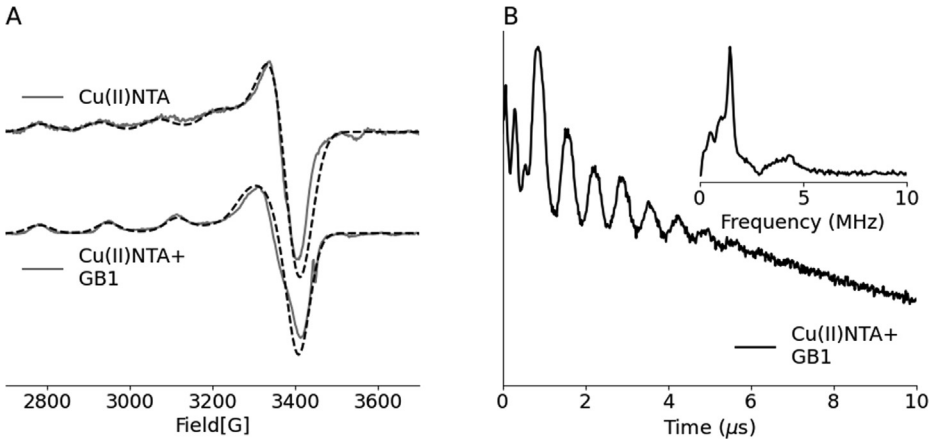

Fig. 5. A) 80 K CW spectra of Cu(II)NTA and Cu(II)NTA + GB1. The dashed lines represent an EasySpin simulation using a single component. Parameters for the simulation are shown in Table S1. B) ESEEM signal of Cu(II)NTA + GB1. The ESEEM spectrum is shown in the inset.

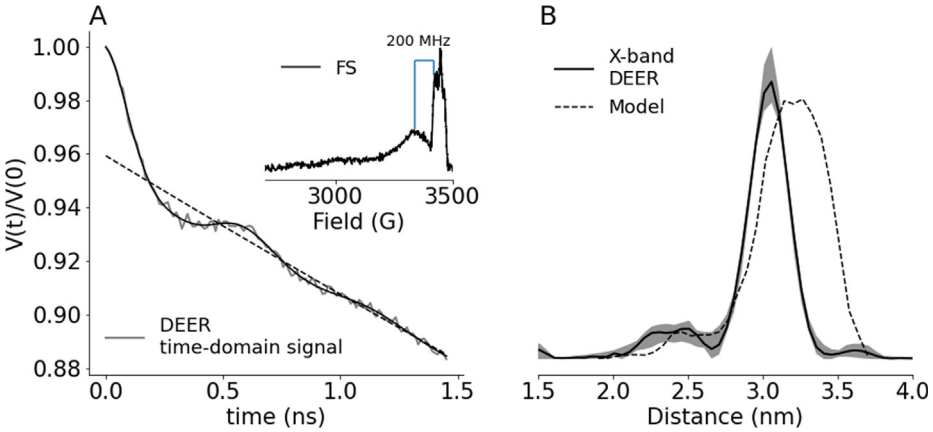

Fig. 6. A) DEER signal of orthogonally-labeled GB1 at 40 K. The time trace was analyzed using CDA [63,64]. The inset shows FS-ESE spectrum of orthogonally-labeled GB1. The blue lines indicate a 200 MHz separation. B) The distance distribution obtained from DEER at 40 K for Cu(II)NTA+$^{13}C_1$-mOX063-d_{24} is shown as the solid line. The shaded gray area represents the error of the distance distribution. For comparison, the predicted distance distribution is overlaid on the experimental distribution.

of Fig. 6A, indicates that the maximum of Cu(II)NTA is ~ 200 MHz away from the first local maximum of the $^{13}C_1$-mOX063-d_{24} spectra. Consequently, we set the observer frequency at the first local maximum of $^{13}C_1$-mOX063-d_{24} and the pump frequency at the maximum of the Cu(II)NTA spectrum in the DEER measurement. We note that setting the pump frequency at $^{13}C_1$-mOX063-d_{24} instead of Cu(II)NTA is possible. However, observing at Cu(II)NTA leads to a smaller DEER echo compared to observing at $^{13}C_1$-mOX063-d_{24}, as shown in Figure S8A. Additionally, if the shot repetition time is not long enough to account for the long T_1 of the pumped $^{13}C_1$-mOX063-d_{24}, the λ is significantly reduced, as shown in Figure S8B. Therefore, observing at the Cu(II)NTA position does not improve the sensitivity of the measurement.

The DEER signal, shown in Fig. 6A, was analyzed using Consensus Deer Analysis [63,64] to obtain the distance distribution. Information on relaxation rates and L-curve is shown in Figures S7 and S8. The DEER distance distribution shows one major distance at 3.0 nm and a minor distribution around 2.5 nm. The minor peak at 2.5 nm was reproducible and was observed in two additional biological repeats. These data are shown in Figure S11.

To understand the distribution, we created an *in silico* model of this orthogonally labeled GB1 mutant. The conformational space of $^{13}C_1$-mOX063-d_{24} was obtained identically to Fig. 4 and previous publication [4]. On the other hand, we got the conformational space of Cu(II)NTA from an MD simulation of GB1 labeled with Cu(II)NTA at K28H/Q32H [73]. The MD simulation was done using previously developed force fields for dHis-Cu(II) [73]. Each frame in the simulation was aligned to the protein to remove any translation or rotation of the complex. As a result, we can visualize the range of position of dHis-Cu(II) with respect to the protein. By combining the conformational space of both Cu(II)NTA and $^{13}C_1$-mOX063-d_{24}, we obtained distance distribution from the *in-silico* model. This predicted distribution is shown in Fig. 6B. From the *in-silico* model, the major distance at 3 nm and the minor distance at 2.5 nm in our experimental distribution are within *in silico* prediction. Details on the minor distribution are explored further in the ESI.

While we measured the distance between Cu(II)NTA and $^{13}C_1$-mOX063-d_{24}, our labeling scheme has the potential for the measurement of multiple distance constraints using X-band DEER experiments. As shown in the inset of Fig. 6A, we only performed DEER with a 200 MHz pulse separation between Cu(II)NTA and $^{13}C_1$-mOX063-d_{24}. However, the spectra also indicate that we can use DEER to obtain distance constraints between two $^{13}C_1$-mOX063-d_{24} or between two Cu(II) labels. As a result, obtaining multiple distance constraints using Cu(II) and TAM-based labels becomes accessible at X-band frequencies.

Measurements between a TAM label and a Cu(II) label have been typically done using RIDME. Because RIDME is a single-frequency experiment, the measurement is more sensitive using

a TAM label with natural abundance of ^{13}C rather than $^{13}C_1$-mOX063-d_{24}. Furthermore, the combination of Cu(II) and TAM has high sensitivity due to the significantly different relaxation rates of the two labels [11,70,74–77]. When performed correctly, RIDME can have a λ close to 50 %, significantly higher than λ of 4 % from our DEER measurement in Fig. 6A. Additionally, RIDME can be done at Q-band as it does not need to account for the separation between the spectra of the two different labels, further improving the sensitivity of the distance measurement. However, RIDME contains a complicated background signal [48] which can complicate the subtraction and analysis procedures [27,47,48,78].

4. Conclusions

In conclusion, this work shows how $^{13}C_1$-mOX063-d_{24} can be easily incorporated into a protein. By taking advantage of the resolved splitting of our label, distance measurements can be performed using DEER at Q-band, which is unfeasible with many other TAM-based labels. Furthermore, this new label can be orthogonally incorporated with dHis-Cu(II) labeling. This facile orthogonal labeling scheme allows for X-band DEER distance measurements. Additionally, the orthogonal labeling scheme has the potential to measure multiple distance constraints with X-band DEER experiments. Together, these results enhance the power of $^{13}C_1$-mOX063-d_{24} for DEER-based distance measurements.

While this work used a unique TAM label that incorporated ^{13}C, the label can be synthesized at a large-scale based on recent works [52,79]. The cost of ^{13}C reagent is negligible in comparison to the whole synthesis. The $^{13}C_1$-mOX063-d_{24} may be even more useful for W-band DEER. At W-band, the breadth of nitroxide is wider than $^{13}C_1$-mOX063-d_{24}. Specifically, the nitroxide spectrum depends on the anisotropy of the g-factor, while the $^{13}C_1$-mOX063-d_{24} spectrum depends on the hyperfine interaction of $^{13}C_1$. Therefore, the sensitivity benefit of $^{13}C_1$-mOX063-d_{24} over nitroxide will be more significant at high frequencies.

Data availability

Data will be made available on request.

Declaration of Competing Interest

The authors declare that they have no known competing financial interests or personal relationships that could have appeared to influence the work reported in this paper.

Acknowledgements

This work was partially supported by NSF-BSF MCB 2001654 to SS and NIH grants: R01EB032321 and R21GM143595 to BD. The content is solely the responsibility of the authors and does not necessarily represent the official views of the National Institutes of Health.

Appendix A. Supplementary material

Supplementary data to this article can be found online at https://doi.org/10.1016/j.jmr.2022.107363.

References

[1] N. Fleck, C. Heubach, T. Hett, S. Spicher, S. Grimme, O. Schiemann, Ox-SLIM: synthesis of and site-specific labelling with a highly hydrophilic trityl spin label, Chem. Eur. J 27 (16) (2021) 5292–5297.
[2] N. Fleck, C.A. Heubach, T. Hett, F.R. Haege, P.P. Bawol, H. Baltruschat, O. Schiemann, SLIM: a short-linked, highly redox-stable trityl label for high-sensitivity in-cell EPR distance measurements, Angew. Chem. Int. Ed. 59 (24) (2020) 9767–9772.
[3] V.M. Tormyshev, A.S. Chubarov, O.A. Krumkacheva, D.V. Trukhin, O.Y. Rogozhnikova, A.S. Spitsyna, A.A. Kuzhelev, V.V. Koval, M.V. Fedin, T.S. Godovikova, et al., Methanethiosulfonate Derivative of OX063 Trityl: a promising and efficient reagent for side-directed spin labeling of proteins, Chem. Eur. J 26 (12) (2020) 2705–2712.
[4] Z. Hasanbasri, K. Singewald, T.D. Gluth, B. Driesschaert, S. Saxena, Cleavage-Resistant protein labeling with hydrophilic trityl enables distance measurements in-cell, J. Phys. Chem. B 125 (20) (2021) 5265–5274.
[5] M. Poncelet, B. Driesschaert, A 13 C-Labeled triarylmethyl radical as an EPR spin probe highly sensitive to molecular tumbling, Angew. Chem. Int. Ed. 59 (38) (2020) 16451–16454.
[6] Z. Yang, M.D. Bridges, C.J. López, O.Y. Rogozhnikova, D.V. Trukhin, E.K. Brooks, V. Tormyshev, H.J. Halpern, W.L. Hubbell, A triarylmethyl spin label for long-range distance measurement at physiological temperatures using T1 relaxation enhancement, J. Magn. Reson. 269 (2016) 50–54.
[7] V.V. Khramtsov, A.A. Bobko, M. Tseytlin, B. Driesschaert, Exchange phenomena in the electron paramagnetic resonance spectra of the nitroxyl and trityl radicals: multifunctional spectroscopy and imaging of local chemical microenvironment, Anal. Chem. 89 (9) (2017) 4758–4771.
[8] G.W. Reginsson, N.C. Kunjir, S.T. Sigurdsson, O. Schiemann, Trityl radicals: spin labels for nanometer-distance measurements, Chem. Eur. J 18 (43) (2012) 13580–13584.
[9] A.A. Kuzhelev, D.V. Trukhin, O.A. Krumkacheva, R.K. Strizhakov, O.Y. Rogozhnikova, T.I. Troitskaya, M.V. Fedin, V.M. Tormyshev, E.G. Bagryanskaya, Room-Temperature electron spin relaxation of triarylmethyl radicals at the X- and Q-Bands, J. Phys. Chem. B 119 (43) (2015) 13630–13640.
[10] R. Owenius, G.R. Eaton, S.S. Eaton, Frequency (250 MHz to 9.2 GHz) and viscosity dependence of electron spin relaxation of triarylmethyl radicals at room temperature, J. Magn. Reson. 172 (1) (2005) 168–175.
[11] A.A. Kuzhelev, O.A. Krumkacheva, G.Y. Shevelev, M. Yulikov, M.V. Fedin, E.G. Bagryanskaya, Room-temperature distance measurements using RIDME and the orthogonal spin labels trityl/nitroxide, Phys. Chem. Chem. Phys. 20 (15) (2018) 10224–10230.
[12] V. Meyer, M.A. Swanson, L.J. Clouston, P.J. Boratyński, R.A. Stein, H.S. Mchaourab, A. Rajca, S.S. Eaton, G.R. Eaton, Room-temperature distance measurements of immobilized spin-labeled protein by DEER/PELDOR, Biophys. J. 108 (5) (2015) 1213–1219.
[13] G.Y. Shevelev, E.L. Gulyak, A.A. Lomzov, A.A. Kuzhelev, O.A. Krumkacheva, M.S. Kupryushkin, V.M. Tormyshev, M.V. Fedin, E.G. Bagryanskaya, D.V. Pyshnyi, A versatile approach to attachment of triarylmethyl labels to DNA for nanoscale structural EPR studies at physiological temperatures, J. Phys. Chem. B 122 (1) (2018) 137–143.
[14] Z. Yang, Y. Liu, P. Borbat, J.L. Zweier, J.H. Freed, W.L. Hubbell, Pulsed ESR dipolar spectroscopy for distance measurements in immobilized spin labeled proteins in liquid solution, J. Am. Chem. Soc. 134 (24) (2012) 9950–9952.
[15] G.Y. Shevelev, O.A. Krumkacheva, A.A. Lomzov, A.A. Kuzhelev, O.Y. Rogozhnikova, D.V. Trukhin, T.I. Troitskaya, V.M. Tormyshev, M.V. Fedin, D.V. Pyshnyi, et al., Physiological-temperature distance measurement in nucleic acid using triarylmethyl-based spin labels and pulsed dipolar EPR spectroscopy, J. Am. Chem. Soc. 136 (28) (2014) 9874–9877.
[16] I. Dhimitruka, A.A. Bobko, T.D. Eubank, D.A. Komarov, V.V. Khramtsov, Phosphonated trityl probes for concurrent in vivo tissue oxygen and pH monitoring using electron paramagnetic resonance-based techniques, J. Am. Chem. Soc. 135 (15) (2013) 5904–5910.
[17] W. Liu, J. Nie, X. Tan, H. Liu, N. Yu, G. Han, Y. Zhu, F.A. Villamena, Y. Song, J.L. Zweier, et al., Synthesis and characterization of pegylated trityl radicals: effect of pegylation on physicochemical properties, J. Org. Chem. 82 (1) (2017) 588–596.
[18] J.J. Jassoy, A. Berndhäuser, F. Duthie, S.P. Kühn, G. Hagelueken, O. Schiemann, Versatile trityl spin labels for nanometer distance measurements on biomolecules in vitro and within cells, Angew. Chem. Int. Ed. 56 (1) (2017) 177–181.
[19] K. Singewald, X. Bogetti, K. Sinha, G.S. Rule, S. Saxena, Double histidine based EPR measurements at physiological temperatures permit site-specific elucidation of hidden dynamics in enzymes, Angew. Chem. Int. Ed. 59 (51) (2020) 23040–23044.
[20] C. Altenbach, C.J. López, K. Hideg, W.L. Hubbell, Exploring structure, dynamics, and topology of nitroxide spin-labeled proteins using continuous-wave electron paramagnetic resonance spectroscopy, Meth. Enzymol. 564 (2015) 59–100.
[21] S. Saxena, J.H. Freed, Theory of double quantum two-dimensional electron spin resonance with application to distance measurements, J. Chem. Phys. 107 (5) (1997) 1317–1340.
[22] P.P. Borbat, J.H. Freed, Multiple-quantum ESR and distance measurements, Chem. Phys. Lett. 313 (1–2) (1999) 145–154.
[23] A.D. Milov, A.G. Maryasov, Y.D. Tsvetkov, Pulsed electron double resonance (PELDOR) and its applications in free-radicals research, Appl Magn Reson 15 (1) (1998) 107–143.
[24] M. Pannier, S. Veit, A. Godt, G. Jeschke, H.W. Spiess, Dead-time free measurement of dipole-dipole interactions between electron spins, J. Magn. Reson. 142 (2) (2000) 331–340.
[25] G. Jeschke, M. Pannier, A. Godt, H.W. Spiess, Dipolar spectroscopy and spin alignment in electron paramagnetic resonance, Chem. Phys. Lett. 331 (2–4) (2000) 243–252.

[26] L.V. Kulik, S.A. Dzuba, I.A. Grigoryev, Y.D. Tsvetkov, Electron dipole–dipole interaction in ESEEM of nitroxide biradicals, Chem. Phys. Lett. 343 (3–4) (2001) 315–324.
[27] S. Milikisyants, F. Scarpelli, M.G. Finiguerra, M. Ubbink, M. Huber, A pulsed EPR method to determine distances between paramagnetic centers with strong spectral anisotropy and radicals: the dead-time free RIDME sequence, J. Magn. Reson. 201 (1) (2009) 48–56.
[28] M. Qi, A. Gross, G. Jeschke, A. Godt, M. Drescher, Gd(III)-PyMTA label is suitable for in-cell EPR, J. Am. Chem. Soc. 136 (43) (2014) 15366–15378.
[29] A. Martorana, G. Bellapadrona, A. Feintuch, E. Di Gregorio, S. Aime, D. Goldfarb, Probing protein conformation in cells by EPR distance measurements using Gd^{3+} spin labeling, J. Am. Chem. Soc. 136 (38) (2014) 13458–13465.
[30] D. Thonon, V. Jacques, J.F. Desreux, A gadolinium triacetic monoamide DOTA derivative with a methanethiosulfonate anchor group. Relaxivity properties and conjugation with albumin and thiolated particles, Contrast Media Mol. Imaging 2 (1) (2007) 24–34.
[31] A. Martorana, Y. Yang, Y. Zhao, Q.-F. Li, X.-C. Su, D. Goldfarb, Mn(II) tags for DEER distance measurements in proteins via C-S attachment, Dalton Trans. 44 (48) (2015) 20812–20816.
[32] D. Banerjee, H. Yagi, T. Huber, G. Otting, D. Goldfarb, Nanometer-range distance measurement in a protein using Mn^{2+} tags, J. Phys. Chem. Lett. 3 (2) (2012) 157–160.
[33] M.J. Lawless, S. Ghosh, T.F. Cunningham, A. Shimshi, S. Saxena, On the use of the Cu2+-iminodiacetic acid complex for double histidine based distance measurements by pulsed ESR, Phys. Chem. Chem. Phys. 19 (31) (2017) 20959–20967.
[34] S. Ghosh, M.J. Lawless, G.S. Rule, S. Saxena, The Cu2+-nitrilotriacetic acid complex improves loading of α-helical double histidine site for precise distance measurements by pulsed ESR, J. Magn. Reson. 286 (2018) 163–171.
[35] T.F. Cunningham, M.R. Putterman, A. Desai, W.S. Horne, S. Saxena, The double-histidine Cu^{2+}-binding motif: a highly rigid, site-specific spin probe for electron spin resonance distance measurements, Angew. Chem. Int. Ed. 54 (21) (2015) 6330–6334.
[36] T.F. Cunningham, M.D. Shannon, M.R. Putterman, R.J. Arachchige, I. Sengupta, M. Gao, C.P. Jaroniec, S. Saxena, Cysteine-specific Cu^{2+} chelating tags used as paramagnetic probes in double electron electron resonance, J. Phys. Chem. B 119 (7) (2015) 2839–2843.
[37] G.Y. Shevelev, O.A. Krumkacheva, A.A. Lomzov, A.A. Kuzhelev, D.V. Trukhin, O. Y. Rogozhnikova, V.M. Tormyshev, D.V. Pyshnyi, M.V. Fedin, E.G. Bagryanskaya, Triarylmethyl labels: toward improving the accuracy of EPR nanoscale distance measurements in dnas, J. Phys. Chem. B 119 (43) (2015) 13641–13648.
[38] J.S. Becker, S. Saxena, Double quantum coherence electron spin resonance on coupled Cu(II)–Cu(II) electron spins, Chem. Phys. Lett. 414 (1–3) (2005) 248–252.
[39] S. Ruthstein, M. Ji, P. Mehta, L. Jen-Jacobson, S. Saxena, Sensitive Cu2+-Cu2+ distance measurements in a protein-DNA complex by double-quantum coherence ESR, J. Phys. Chem. B 117 (20) (2013) 6227–6230.
[40] S. Ruthstein, M. Ji, B.-K. Shin, S. Saxena, A simple double quantum coherence ESR sequence that minimizes nuclear modulations in Cu(2+)-ion based distance measurements, J. Magn. Reson. 257 (2015) 45–50.
[41] M. Bonora, J. Becker, S. Saxena, Suppression of electron spin-echo envelope modulation peaks in double quantum coherence electron spin resonance, J. Magn. Reson. 170 (2) (2004) 278–283.
[42] A. Meyer, J.J. Jassoy, S. Spicher, A. Berndhäuser, O. Schiemann, Performance of PELDOR, RIDME, SIFTER, and DQC in measuring distances in trityl based bi- and triradicals: exchange coupling, pseudosecular coupling and multi-spin effects, Phys. Chem. Chem. Phys. 20 (20) (2018) 13858–13869.
[43] N.C. Kunjir, G.W. Reginsson, O. Schiemann, S.T. Sigurdsson, Measurements of short distances between trityl spin labels with CW EPR, DQC and PELDOR, Phys. Chem. Chem. Phys. 15 (45) (2013) 19673–19685.
[44] J.J. Jassoy, C.A. Heubach, T. Hett, F. Bernhard, F.R. Haege, G. Hagelueken, O. Schiemann, Site selective and efficient spin labeling of proteins with a maleimide-functionalized trityl radical for pulsed dipolar EPR spectroscopy, Molecules 24 (15) (2019).
[45] D. Akhmetzyanov, P. Schöps, A. Marko, N.C. Kunjir, S.T. Sigurdsson, T.F. Prisner, Pulsed EPR dipolar spectroscopy at Q- and G-band on a trityl biradical, Phys. Chem. Chem. Phys. 17 (37) (2015) 24446–24451.
[46] O.A. Krumkacheva, G.Y. Shevelev, A.A. Lomzov, N.S. Dyrkheeva, A.A. Kuzhelev, V.V. Koval, V.M. Tormyshev, Y.F. Polienko, M.V. Fedin, D.V. Pyshnyi, et al., DNA complexes with human apurinic/apyrimidinic endonuclease 1: structural insights revealed by pulsed dipolar EPR with orthogonal spin labeling, Nucleic Acids Res. 47 (15) (2019) 7767–7780.
[47] I. Ritsch, H. Hintz, G. Jeschke, A. Godt, M. Yulikov, Improving the accuracy of Cu (ii)-nitroxide RIDME in the presence of orientation correlation in water-soluble Cu(ii)-nitroxide rulers, Phys. Chem. Chem. Phys. 21 (19) (2019) 9810–9830.
[48] A.V. Astashkin, Mapping the Structure of Metalloproteins with RIDME, Meth. Enzymol. 563 (2015) 251–284.
[49] A. Giannoulis, Y. Yang, Y.-J. Gong, X. Tan, A. Feintuch, R. Carmieli, T. Bahrenberg, Y. Liu, X.-C. Su, D. Goldfarb, DEER distance measurements on trityl/trityl and Gd(iii)/trityl labelled proteins, Phys. Chem. Chem. Phys. 21 (20) (2019) 10217–10227.
[50] Y. Yang, B.-B. Pan, X. Tan, F. Yang, Y. Liu, X.-C. Su, D. Goldfarb, In-Cell Trityl-Trityl distance measurements on proteins, J. Phys. Chem. Lett. 11 (3) (2020) 1141–1147.
[51] A.A. Kuzhelev, V.M. Tormyshev, O.Y. Rogozhnikova, D.V. Trukhin, T.I. Troitskaya, R.K. Strizhakov, O.A. Krumkacheva, M.V. Fedin, E.G. Bagryanskaya, Triarylmethyl radicals: EPR study of 13C hyperfine coupling constants, Z Phys Chem (N F) 231 (4) (2017) 777–794.
[52] M. Poncelet, T. Ngendahimana, T.D. Gluth, E.H. Hoblitzell, T.D. Eubank, G.R. Eaton, S.S. Eaton, B. Driesschaert, Synthesis and characterization of a biocompatible 13C1 isotopologue of trityl radical OX071 for in vivo EPR viscometry, Analyst 147 (24) (2022) 5643–5648.
[53] T.F. Cunningham, M.S. McGoff, I. Sengupta, C.P. Jaroniec, W.S. Horne, S. Saxena, High-resolution structure of a protein spin-label in a solvent-exposed β-sheet and comparison with DEER spectroscopy, Biochemistry 51 (32) (2012) 6350–6359.
[54] K. Singewald, J.A. Wilkinson, A.S. Saxena, Copper based site-directed spin labeling of proteins for use in pulsed and continuous wave EPR spectroscopy, Bio Protoc 11 (24) (2021) e4258.
[55] A. Gamble Jarvi, J. Casto, S. Saxena, Buffer effects on site directed Cu2+-labeling using the double histidine motif, J. Magn. Reson. 320 (2020).
[56] W.B. Mims, Envelope modulation in spin-echo experiments, Phys. Rev. B 5 (7) (1972) 2409–2419.
[57] W.B. Mims, Amplitudes of superhyperfine frequencies displayed in the electron-spin-echo envelope, Phys. Rev. B 6 (9) (1972) 3543–3545.
[58] S.A. Dikanov, Y. Tsvetkov, Electron spin echo envelope modulation (ESEEM) spectroscopy, CRC Press, 1992.
[59] A.M. Gronenborn, D.R. Filpula, N.Z. Essig, A. Achari, M. Whitlow, P.T. Wingfield, G.M. Clore, A novel, highly stable fold of the immunoglobulin binding domain of streptococcal protein G, Science 253 (5020) (1991) 657–661.
[60] T.F. Cunningham, S. Pornsuwan, W.S. Horne, S. Saxena, Rotameric preferences of a protein spin label at edge-strand β-sheet sites, Protein Sci. 25 (5) (2016) 1049–1060.
[61] S. Stoll, A. Schweiger, EasySpin, a comprehensive software package for spectral simulation and analysis in EPR, J. Magn. Reson. 178 (1) (2006) 42–55.
[63] S.G. Worswick, J.A. Spencer, G. Jeschke, I. Kuprov, Deep neural network processing of DEER data, Sci. Adv. 4 (8) (2018) eaat5218.
[64] L. Fábregas Ibáñez, G. Jeschke, S. Stoll, DeerLab: a comprehensive software package for analyzing dipolar electron paramagnetic resonance spectroscopy data, Magn. Reson. 1 (2) (2020) 209–224.
[65] G. Hagelueken, R. Ward, J.H. Naismith, O. Schiemann, MtsslWizard. In Silico Spin-Labeling and Generation of Distance Distributions in PyMOL, Appl Magn Reson 42 (3) (2012) 377–391.
[66] Z. Yang, M. Ji, S. Saxena, Practical Aspects of Copper Ion-Based Double Electron Electron Resonance Distance Measurements, Appl Magn Reson 39 (4) (2010) 487–500.
[67] Y.D. Tsvetkov, A.D. Milov, A.G. Maryasov, Pulsed electron–electron double resonance (PELDOR) as EPR spectroscopy in nanometre range, Russian Chem. Rev. (2008).
[68] B.E. Bode, D. Margraf, J. Plackmeyer, G. Dürner, T.F. Prisner, O. Schiemann, Counting the monomers in nanometer-sized oligomers by pulsed electron-electron double resonance, J. Am. Chem. Soc. 129 (21) (2007) 6736–6745.
[69] A.D. Milov, A.B. Ponomarev, Y.D. Tsvetkov, Electron-electron double resonance in electron spin echo: model biradical systems and the sensitized photolysis of decalin, Chem. Phys. Lett. 110 (1) (1984) 67–72.
[70] J.L. Wort, K. Ackermann, A. Giannoulis, A.J. Stewart, D.G. Norman, B.E. Bode, Sub-Micromolar pulse dipolar EPR spectroscopy reveals increasing CuII -labelling of double-histidine motifs with lower temperature, Angew. Chem. Int. Ed. 58 (34) (2019) 11681–11685.
[71] J. McCracken, J. Peisach, D.M. Dooley, Cu(II) coordination chemistry of amine oxidases. Pulsed EPR studies of histidine imidazole, water, and exogenous ligand coordination, J. Am. Chem. Soc. 109 (13) (1987) 4064–4072.
[72] K.I. Silva, B.C. Michael, S.J. Geib, S. Saxena, ESEEM analysis of multi-histidine Cu (II)-coordination in model complexes, peptides, and amyloid-β, J. Phys. Chem. B 118 (30) (2014) 8935–8944.
[73] X. Bogetti, S. Ghosh, A. Gamble Jarvi, J. Wang, S. Saxena, Molecular dynamics simulations based on newly developed force field parameters for Cu^{2+} spin labels provide insights into double-histidine-based double electron-electron resonance, J. Phys. Chem. B 124 (14) (2020) 2788–2797.
[74] A. Giannoulis, C.L. Motion, M. Oranges, M. Bühl, G.M. Smith, B.E. Bode, Orientation selection in high-field RIDME and PELDOR experiments involving low-spin CoII ions, Phys. Chem. Chem. Phys. 20 (4) (2018) 2151–2154.
[75] A. Meyer, D. Abdullin, G. Schnakenburg, O. Schiemann, Single and double nitroxide labeled bis(terpyridine)-copper(II): influence of orientation selectivity and multispin effects on PELDOR and RIDME, Phys. Chem. Chem. Phys. 18 (13) (2016) 9262–9271.
[76] J.L. Wort, S. Arya, K. Ackermann, A.J. Stewart, B.E. Bode, Pulse Dipolar EPR reveals double-histidine motif CuII-NTA spin-labeling robustness against competitor ions, J. Phys. Chem. Lett. 12 (11) (2021) 2815–2819.
[77] A. Giannoulis, M. Oranges, B.E. Bode, Monitoring complex formation by relaxation-induced pulse electron paramagnetic resonance distance measurements, ChemPhysChem 18 (17) (2017) 2318–2321.
[78] D. Abdullin, F. Duthie, A. Meyer, E.S. Müller, G. Hagelueken, O. Schiemann, Comparison of PELDOR and RIDME for Distance Measurements between Nitroxides and Low-Spin Fe(III) Ions, J. Phys. Chem. B 119 (43) (2015) 13534–13542.
[79] M. Poncelet, J.L. Huffman, V.V. Khramtsov, I. Dhimitruka, B. Driesschaert, Synthesis of hydroxyethyl tetrathiatriarylmethyl radicals OX063 and OX071, RSC Adv. 9 (60) (2019) 35073–35076.